

Probing Embryonic Development Enables the Discovery of Unique Small-Molecule Bone Morphogenetic Protein Potentiators

Fabian Wessler, Daniel Riege, Mahesh Puthanveedu, Jonas Halver, Eva Müller, Jessica Bertrand, Andrey P. Antonchick, Sonja Sievers, Herbert Waldmann, and Dennis Schade*



Cite This: <https://doi.org/10.1021/acs.jmedchem.1c01800>



Read Online

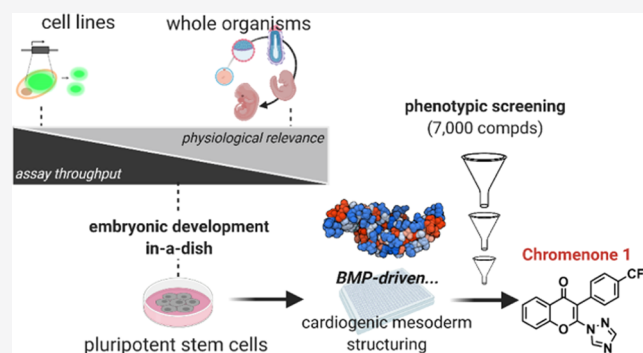
ACCESS |

Metrics & More

Article Recommendations

Supporting Information

ABSTRACT: We report on the feasibility to harness embryonic development *in vitro* for the identification of small-molecule cytokine mimetics and signaling activators. Here, a phenotypic, target-agnostic, high-throughput assay is presented that probes bone morphogenetic protein (BMP) signaling during mesodermal patterning of embryonic stem cells. The temporal discrimination of BMP- and transforming growth factor- β (TGF β)-driven stages of cardiomyogenesis underpins a selective, authentic orchestration of BMP cues that can be recapitulated for the discovery of BMP activator chemotypes. Proof of concept is shown from a chemical screen of 7000 compounds, provides a robust hit validation workflow, and afforded 2,3-disubstituted 4H-chromen-4-ones as potent BMP potentiators with osteogenic efficacy. Mechanistic studies suggest that Chromenone 1 enhances canonical BMP outputs at the expense of TGF β -Smads in an unprecedented manner. Pharmacophoric features were defined, providing a set of novel chemical probes for various applications in (stem) cell biology, regenerative medicine, and basic research on the BMP pathway.



INTRODUCTION

Bone morphogenetic proteins (BMPs) belong to the superfamily of transforming growth factor- β (TGF β) ligands and play central roles during embryonic development, tissue homeostasis, and regeneration.^{1,2} The quality and quantity of BMP signaling outputs largely depend on the cellular context and are regulated at multiple levels. Typically, dimeric BMP ligands bring the type I (i.e., ALK-1, -2, -3, -6) and constitutively active type II (i.e., BMRP-II, ActR-II, ActR-IIB) BMP receptors into close proximity, inducing transphosphorylation of the type I receptor, which in turn activates BMP-Smads (i.e., Smads-1, -5, -9).^{3,4} These receptor-activated, phosphorylated R-Smads form a complex with Smad4, which translocates to the nucleus, leading to the expression of canonical BMP target genes [e.g., inhibitor of DNA binding (Id) gene family].⁵ However, many downstream effects of BMPs are not mediated by Smad but noncanonical pathways (e.g., PI3K/Akt, Erk, MAPK) and both signaling cascades are regulated at various levels.²

Owing to their pronounced osteoinductive activity, BMPs mostly gained attention for therapeutic approaches to address skeletal trauma and osteopenic diseases,^{1,6} which present an enormous challenge for the health and economic system, particularly in view of our demographic changes. Recombinant BMPs are in clinical use to support treatment of difficult fractures but need to be administered at doses 10 000-fold

beyond physiological concentrations, which is not only costly but associated with adverse effects (e.g., inflammation, heterotopic ossification).^{6,7}

Hence, chemical modalities that serve as genuine mimetics or potentiators of BMP signaling are highly desirable. In general, a BMP-mimetic molecule (i.e., activator) would be able to activate signaling in the absence of BMP ligand, whereas potentiators enhanced cellular downstream outputs of BMPs. Exciting examples have been reported, including Ventromorphin,⁸ PD-407824, and the recently developed FK506 derivatives,^{9,10} the latter of which highlighted therapeutic applications beyond bone regeneration, i.e., for the treatment of acute kidney injury. However, the discovery and development of novel small-molecule growth factor/cytokine activators are intrinsically challenging. Classic screening approaches utilized reporter gene assays in immortalized cell lines to identify BMP activators but might miss attractive compound hits and targets due to a lack of authentic BMP pathway regulation. On the other hand, physiologically more

Received: October 20, 2021

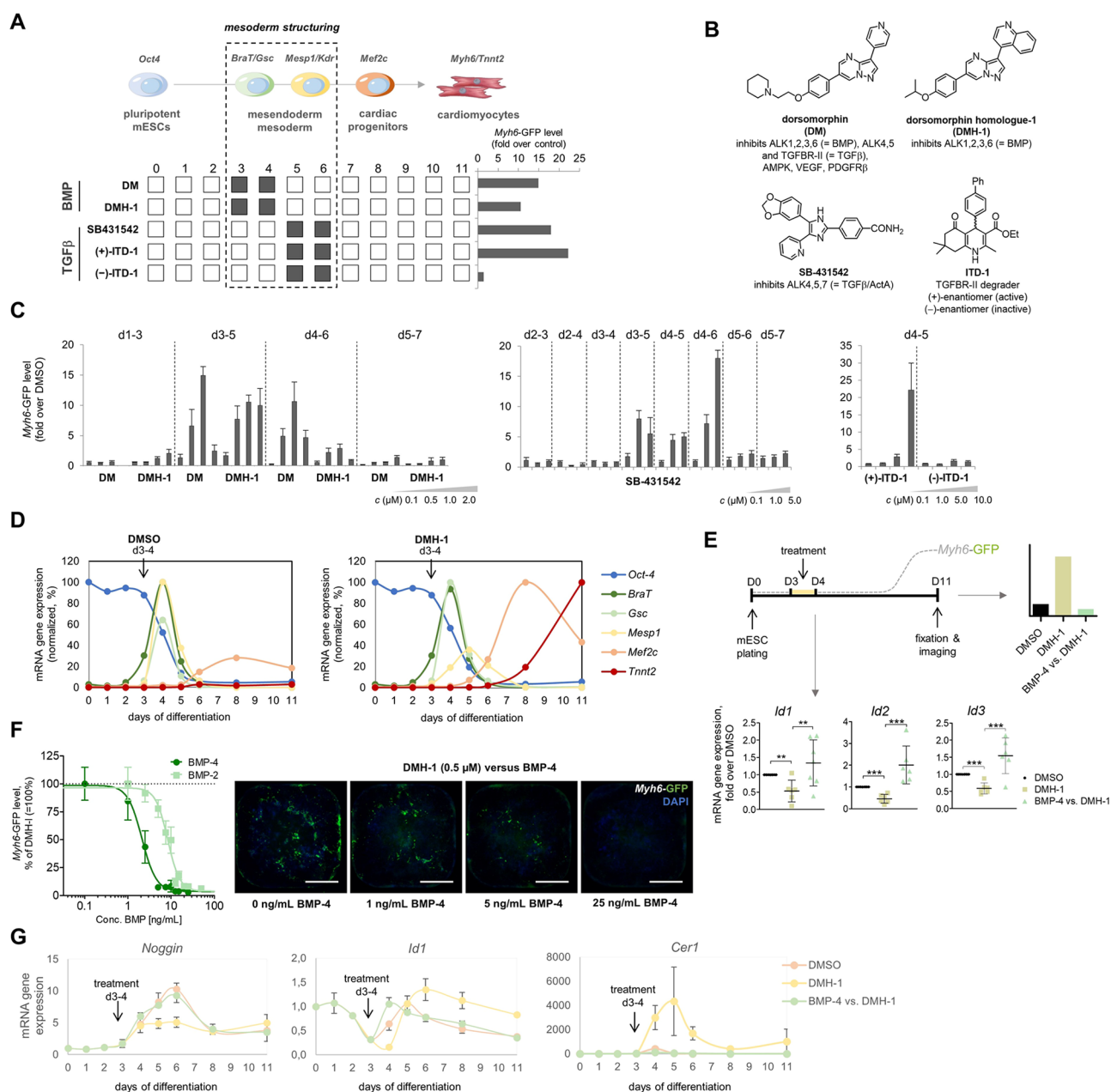


Figure 1. Assessment of BMP signaling during mesoderm structuring enables phenotypic screening for BMP activators. (A) Cardiopoietic differentiation from pluripotent ES cells is illustrated on the basis of cell state-specific markers; cardiac differentiation of mESC-Myh6-GFP in 384-well format upon exposure to TGF β /BMP inhibitors during mesoderm structuring (days 3–6); GFP $^{+}$ -cardiomyocytes are quantified by high-content imaging on day 11 [normalized to dimethylsulfoxide (DMSO) vehicle controls]. (B) Chemical structures of TGF β /BMP signaling inhibitors used as a toolset to probe mesodermal patterning. (C) Dose-dependent profiling of TGF β /BMP inhibitors during the course of mESC differentiation identifies day 3–4 as a BMP-selective time window for cardiogenesis: BMP inhibitors DM and DMH-1 were exposed to cells for 48 h and TGF β -inhibitor SB-431542 for 24 and 48 h and at the indicated time frames; active and inactive enantiomers of the TGF β -inhibitor ITD-1 were tested in the TGF β -specific time window for 24 h. Data are normalized to DMSO and shown as mean \pm standard error of the mean (SEM). (D) DMH-1 stimulates mesodermal structuring toward cardiovascular progenitors: Temporal mRNA expression profiles of cell-specific markers during spontaneous mESC differentiation (DMSO) and DMH-1 (0.5 μ M) treatment in the BMP-sensitive d3–4-time frame; RNA was isolated after 24 h treatments and transcripts were quantified by quantitative real-time polymerase chain reaction (qRT-PCR); data are shown as mean \pm standard deviation (SD) ($n = 3$), normalized to the maximum expression of each gene (=100%). (E) Schematic representation of the screening assay setup for the identification of BMP activators by rescue of DMH-1-induced (0.5 μ M) cardiogenesis in mESC-Myh6-GFP; functional rescue by BMP-4 (10 ng/mL) is confirmed by relative quantification of *Id1*, *Id2*, *Id3* gene expressions (qRT-PCR) after DMH-1/BMP-4 co-treatment for 24 h between d3–4; data are shown as mean \pm SEM ($n = 6–7$, normalized to DMSO), statistical significance was calculated by unpaired *t*-tests ($*p < 0.05$; $**p < 0.01$; $***p < 0.001$). (F) DMH-1-induced (0.5 μ M) cardiogenesis in mESC-Myh6-GFP is antagonized by BMP-2 and -4 between days 3 and 4 in a dose-dependent manner. Representative images show total (DAPI $^{+}$) and cardiac cells (GFP $^{+}$ /DAPI $^{+}$); scale bar = 1 mm. (G) DMH-1 perturbs direct BMP effectors and induces the expression of Cerberus-1: Temporal qRT-PCR profiles depict the expression of canonical BMP target genes *Noggin*, *Id1*, and the master regulator of Nodal/BMP *Cer-1* upon treatment with DMH-1 (0.5 μ M) and co-treatment with BMP-4 (10 ng/mL) between d3–4 of mESC differentiation; data are shown as mean \pm SD ($n = 3$, normalized to day 0 for each treatment).

relevant *in vivo* screens (e.g., in zebrafish) do not allow testing high numbers of compounds and are prone to capture multiple pathways.

Here, we aimed at devising a physiological, morphogenic cellular screening system that is focused on the BMP pathway, yet target-agnostic, to increase chances for expanding the druggable space of potential BMP effectors. In this regard, embryonic stem cells (ESCs) represent a highly attractive option as they have the potential to form almost all cell types of an organism. Fundamental mechanisms of cell fate decisions have been studied to unravel and dissect the involved signaling pathways on the molecular level. Building on this knowledge, our chemical biology-driven approach identified a specific, BMP-dependent time frame during mesodermal structuring of murine ESCs toward cardiovascular cell fates. This discovery enabled probing of the BMP pathway in a high-throughput (HT) manner, screening a chemical library of 7000 compounds. A panel of secondary, orthogonal BMP-dependent assays established stringent filtering and validation criteria. These efforts furnished 4*H*-chromen-4-ones as a novel osteogenic BMP activator chemotype that potentiated BMP signaling outputs in an unprecedented manner via negative TGF β feedback loops, independent of direct kinase inhibition.

Our results highlight the potential of the herein presented stem cell-based system to identify novel BMP activator modalities for various applications in (stem cell) biotechnology, regenerative medicine, and basic research on the BMP pathway. To the best of our knowledge, harnessing embryonic development *in vitro* has not been reported previously for pathway-targeted, phenotypic drug discovery.

RESULTS AND DISCUSSION

Chemical Biology Approach Dissects BMP Dynamics during Mesoderm Patterning, Enabling Phenotypic Screening for Signaling Activators. BMPs play multiple roles during embryogenesis that differ among species and depend on developmental states. While BMP-4 supports self-renewal via inhibition of noncanonical effectors p38 and ERK in murine but not in human pluripotent stem cells (PSCs), it serves, together with Wnt/ β -Catenin, as an effective driver of mesoderm induction in human PSCs.^{11–13} The latter feature is widely utilized for Xeno-free, directed differentiation protocols to generate mesoderm-derived cells such as cardiomyocytes or endothelial cells.^{11,14,15} In this regard, BMP signaling plays multiphasic roles as it is not only key to form mesoderm but is involved in the specification of mesodermal cells to cardiovascular progenitors and later necessary for cardiac induction.^{16,17} In differentiating mESCs, it has been shown that Nodal and BMP must be inhibited individually for progenitors to differentiate toward cardiogenic mesoderm (days 3–5), while at later stages (days 5–7), BMP is required again for cardiac progenitor differentiation.^{16,18,19} Concrete timings typically rely on the differentiation techniques employed (e.g., in two-dimensional (2D) or three-dimensional (3D)/embryoid body-formats). The Mercola group found that combinations of the small-molecule BMP inhibitor dorsomorphin (DM)²⁰ and the TGF β /Activin A inhibitor SB-431542 during mesoderm patterning synergistically enhanced cardiac differentiation when used at optimal low doses.¹⁶ However, DM also potentially affects TGF β /Activin A (and other growth factor pathways) creating redundancy with the activity of SB-431542.

Here, we questioned whether it is possible to differentially probe specific members of the TGF β superfamily during mESC differentiation using high-quality chemical probes. To do this, the ALK-1,-2,-3-selective dorsomorphin-homologue 1 (DMH-1)²¹ was used and compared with DM, the ALK4,5,7 inhibitor SB-431542, and the TGF β -selective TGFBR-II degrader ITD-1^{22,23} after early mesoderm formation (i.e., after day 3 of differentiation). Image-based quantification of *Myh6*-GFP⁺ clusters, which are indicative for early cardiomyocyte formation, suggested that selective BMP inhibition by DMH-1 does not stimulate cardiac differentiation as effectively as observed for the TGF β inhibitors (+)-ITD-1 (i.e., active (+)-enantiomer) and SB-431542 (Figure 1A). Importantly, Figure 1C shows that DMH-1 effectively promoted differentiation already at 0.5 μ M when administered between d3–5 while being almost entirely inactive between d4–6. The pan-ALK inhibitor DM was comparably active between d3–5 and d4–6 of mESC differentiation due to the overlapping inhibition of TGF β . In line with this data, the ALK-4,-5,-7 inhibitor SB-431542 enhanced cardiac differentiation most effectively between d4–6 but was entirely inactive between d3–4.

Given that days 3–4 appeared to be particularly responsive to BMP signaling, we assessed consequences on ESC differentiation toward cardiac fates. Gene expression analysis of specific developmental state and cell markers substantiated that DMH-1 treatment between d3–4 indeed affected mesoderm structuring by timely shifting and reducing the formation of *Mesp1* progenitors, enhancing *Mef2c* cardiac progenitors, and consequently, *Tnnt2* cardiomyocytes (Figure 1D). Thus, the cardiogenic activity of selective BMP inhibition in this time frame likely reflects the fact that *Mesp1*+ mesendodermal progenitors contribute to a range of non-cardiac cells.¹⁷

In view of our original aim to develop an assay that identifies BMP activators, we next tested whether the low-dose BMP blockade by DMH-1 can be antagonized and possibly fully rescued by exogenous BMP addition. Since *Id1,2* and *Id3* represent the key downstream target genes of the BMP pathway that are critically involved in cardiac differentiation,¹⁶ we monitored their expression signatures during cardiogenic mesoderm patterning. Indeed, DMH-1-mediated inhibition of *Id1,2* and *Id3* gene expression was effectively restored by 10 ng/mL BMP-4 (Figure 1E). Accordingly, cardiac differentiation as the ultimate phenotypic screening readout was completely inhibited in a dose-dependent manner without affecting total cell numbers (Figure 1E,F). We used BMP-4 as it plays a major role in embryonic development, but also BMP-2 was able to reverse the selective DMH-1-induced phenotype, albeit at higher doses (Figure 1F). To further emphasize the specificity and functionality of this regulatory circuit, the addition of the endogenous BMP inhibitor Noggin again reverted BMP-4/DMH-1 phenotypes (Figure S1H). We also determined that the BMP target gene *Id1* follows its characteristic multiphasic expression patterns and is upregulated between d3–4 during spontaneous mESC differentiation (Figure 1G). DMH-1 treatment effectively blocked this effect and induced a shift of *Id1* expression toward later stages. Again, this perturbation could be fully rescued by co-administration of BMP-4. Interestingly, the endogenous BMP inhibitor Noggin was not directly perturbed upon DMH-1 treatment but rather remained static at d4 *Noggin* expression levels. The secreted protein Cerberus is required for the transition of uncommitted

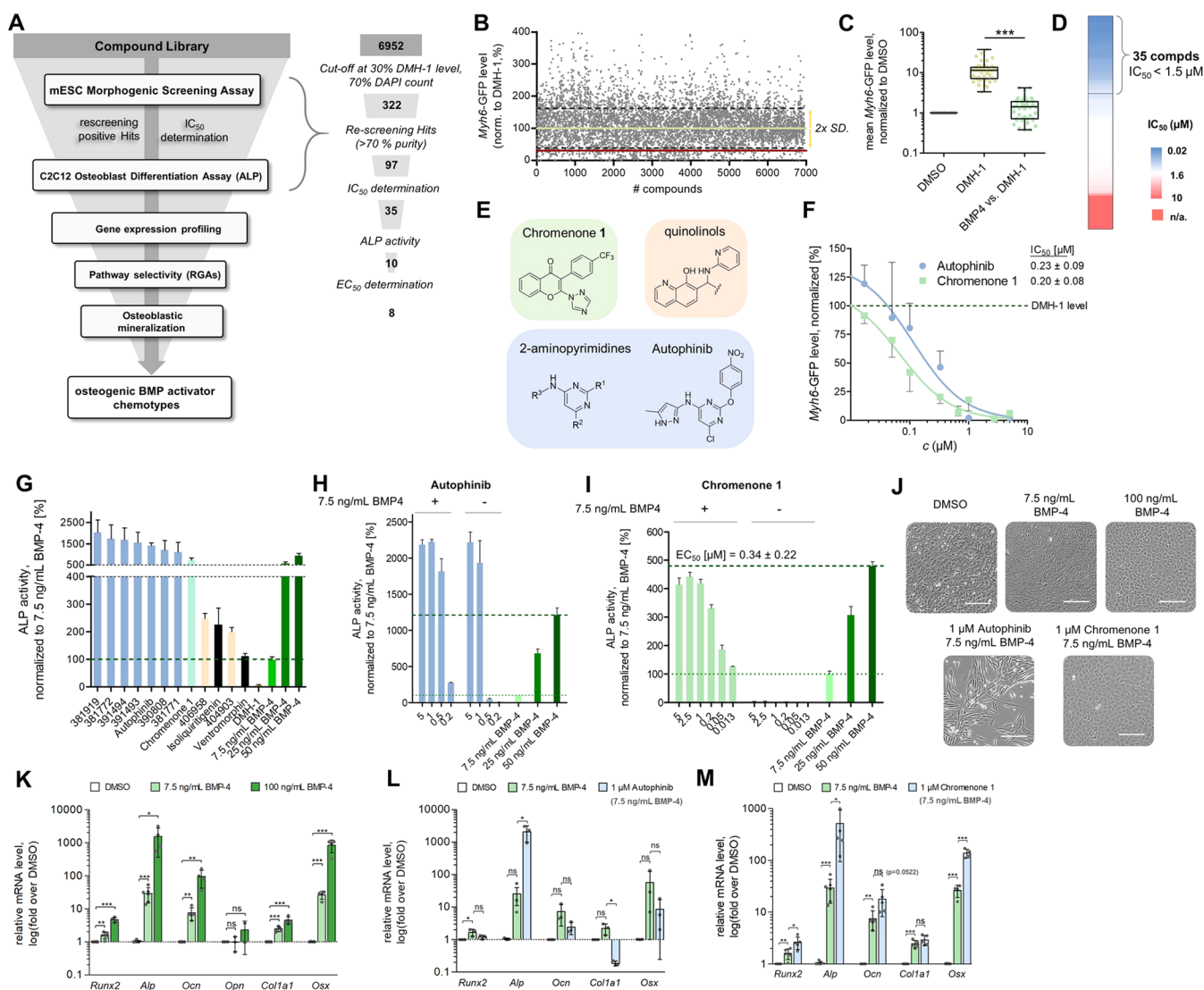


Figure 2. Screening of a diversity-focused compound library and orthogonal assay panel yields Chromenone 1 as a novel osteogenic BMP potentiator. (A) Illustration of screening and validation workflows to identify osteogenic BMP activators: 1° screening was done in mESCs and IC₅₀-validated hits moved forward to 2° screening in C2C12 cells, furnishing three distinct chemotypes of putative osteogenic BMP activators for mechanistic validation via gene expression analysis (C2C12), pathway selectivity (reporter gene assays, RGAs), and osteoblast mineralization (human SaOS-2 cells). (B–D) Summary of HT-screening results in mESC-Myh6-GFP: Cells were exposed to library compounds (5 μM) together with DMH-1 (0.5 μM) for 24 h at d3–4 of differentiation; data are normalized to DMH-1 (=100%, green line), the red line indicates the threshold for hit selection (= <30% Myh6-GFP); dynamic range of mESC screening assay (C) was 10-fold for the induction (=DMH-1) and antagonism (=DMH-1/BMP-4) of BMP-driven cardiogenesis. Data are shown as mean ± SD Myh6-GFP levels under screening conditions (*n* = 45 plates); statistical analysis was performed with an unpaired *t*-test (***p* < 0.01). Dose-dependency hit validation (D) yields 35 potent inhibitors with IC₅₀'s < 1.5 μM. n/a, not applicable. (E) Chemical structures of the three identified active BMP activator chemotypes. (F) Dose–response profiles of Autophinib and Chromenone 1 display high potencies and efficacies as BMP-4-mimetics on DMH-1-induced (0.5 μM) mESC-Myh6-GFP cardiogenesis. Data are shown as mean ± SEM (*n* = 3). (G–I) Effects of screening hits and controls (=Isoliquiritigenin, Ventromorphin) on C2C12 osteoblast differentiation at single doses (G, 5 μM) and dose-dependently for Autophinib and Chromenone 1 (H, I), compared to low- (7.5 ng/mL), medium- (50 ng/mL), and high-dosed (100 ng/mL) BMP-4; data are shown as mean ± SD ALP activity (*n* ≥ 3), normalized to 7.5 ng/mL BMP-4 (=100%). (J) Representative micrographs reveal distinct morphologies of BMP-4 and Chromenone 1/BMP-4-treated C2C12 cells after 72 h compared to Autophinib (scale bar = 200 μm). (K–M) Relative quantification of BMP-dependent osteogenic gene expression transcripts confirmed Chromenone 1 as a BMP-4 potentiator: C2C12 cells were treated with DMSO vehicle control, BMP-4 (7.5 ng/mL) in the presence or absence of compound (1 μM) for 72 h; data are shown as mean ± SD (*n* ≥ 3) and compared to DMSO. Statistical analysis was performed with an unpaired two-tailed *t*-test (**p* < 0.05; ***p* < 0.01; ****p* < 0.001).

to committed cardiac progenitor cells by a coordinated inhibition of BMP and Nodal.^{16,24} Thus, we followed *Cerberus 1* (*Cer1*) expression and found that it was substantially induced and shifted from d4 peak levels toward d5–6 of differentiation, explaining the pronounced Myh6 cardiogenic effect of DMH-1. The physiological expression patterns of both *Noggin* and *Cer1*

could be once more restored when BMP-4 is added to DMH-1 treatments (Figure 1G).

Notably, side-by-side comparison of a series of BMP/ALK-inhibitors suggested that primarily targeting of ALK-3 (BMPRIA) affects cardiogenic differentiation since the highly ALK-2 (ACVR1)-selective ML347²⁵ was only active at

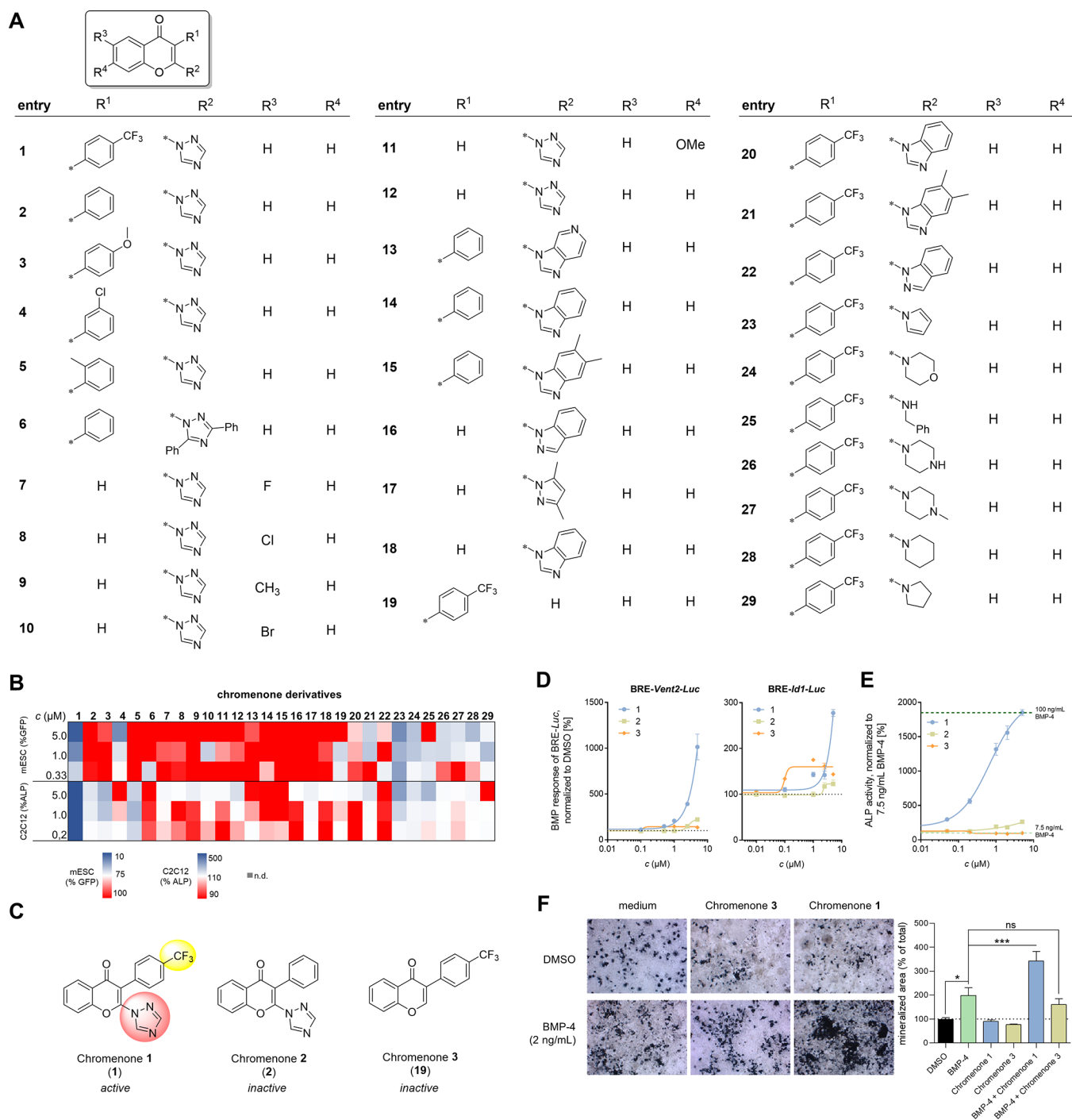


Figure 3. Structure–activity relationship studies furnish a set of chromenone-type chemical probes as BMP activators that enhance human SaOS-2 mineralization *in vitro*. (A) Synthesized series of chromenone derivatives 1–29. (B) Comparative activity profiling of 29 chromenone derivatives at three concentrations in the BMP-dependent mESC- and C2C12 differentiation assays. Heatmap representation of activity data shows mean values of $n \geq 3$ independent experiments. (C) Chemical structures of Chromenone 1–3 highlight key pharmacophoric features in 2- and 3-position required for BMP activity. (D) Dose-dependent profiles of Chromenones 1–3 on BMP-response element (BRE) firefly luciferase reporters using the *Vent2* and *Id1* promoters; BRE-*luc* reporter activity was analyzed in transiently transfected 293T cells after 22 h co-treatment with compounds and BMP-4 (10 ng/mL). (E) BMP-synergistic ALP activation profiles of Chromenones 1–3 in C2C12 underlined high potency ($EC_{50} = 0.34 \mu\text{M}$) and efficacy (ca. 13-fold over low-dosed BMP-4) of Chromenone 1 compared to the inactive Chromenones 2–3. (F) Chromenone 1 induced osteoblastic mineralization in human osteosarcoma cell line (SaOS-2) after 11 days of osteogenic differentiation; von Kossa staining was used for image-based quantification of mineralization; bar graphs depict data as mean \pm SEM ($n = 9$). Statistical analysis was performed using one-way analysis of variance (ANOVA) test ($*p < 0.05$, $**p < 0.01$, $***p < 0.001$).

concentrations far beyond its ALK-2 IC_{50} value of 32 nM (i.e., 2.7 μM , >80-fold) (Figure S1E,F). Given that ALK-2 is the only receptor able to mediate Activin/Nodal induction of BMP

signaling,^{26,27} it appears that we can recapitulate BMPR-I/II-dependent BMP signaling quite selectively during mesodermal patterning.

Collectively, these data underscored that days 3–4 of differentiation are indicative of BMP signaling and that BMP can be discriminated from the TGF β /ActA pathways. These findings served as a promising starting point to develop a high-throughput (HT)-compatible system that enables screening for compounds that mimic the herein demonstrated, specific BMP-4-mediated blockade of cardiogenesis by the BMP inhibitor DMH-1.

Several technical hurdles were tackled for robust screening, including optimal fetal bovine serum (FBS) and DMSO (vehicle) concentrations, and a minimal number of media changes to facilitate HT-workflows throughout the 11-day differentiation period (Figure S1). All HT-robotics and liquid handling steps were well tolerated. Automated microscopy was optimized based on our established procedures to accelerate image acquisition, and thus, screening tempo (Figure S1D).^{22,23,28} The literature-known small-molecule BMP activators/potentiators Isoliquiritigenin,²⁹ Ventromorphan,⁸ and PD-407824⁹ were profiled as positive controls (Figure S1G).

Orthogonal Hit Validation Established Chromenone 1 as a Novel Osteogenic BMP Activator Chemotype.

The established phenotypic BMP assay in mESCs was used to screen an in-house, diversity-focused library of almost 7000 compounds and selected hits that reduced the DMH-1-induced cardiogenesis within a typical 10-fold dynamic range below 30% (i.e., >2-fold the SD) without decreasing total cell numbers (i.e., >70% 4',6-diamidino-2-phenylindole, DAPI counts) (Figure 2A–C). Confirmatory re-screening left 97 hits from which 35 (i.e., 0.5% hit rate) exhibited decent dose–response profiles with IC₅₀'s below 1.5 μ M (Figure 2A,D). For further validation, an orthogonal assay was employed that quantifies BMP-dependent osteoblast differentiation from C2C12 myoblasts (Figure 2A, assay details in Figure S2). A total of 10 compounds robustly stimulated osteoblastogenesis, resembling three distinct chemotypes that comprised two quinolinols, one 4H-chromen-4-one (Chromenone 1), and seven 2-aminopyrimidines (Figure 2E,G). Subsequent evaluation of several quinolinol derivatives could not confirm this hit class (Figure S4). However, the 2-aminopyrimidine Autophinib and Chromenone 1 rescued DMH-1-induced cardiogenesis about equally potent (IC₅₀'s = 0.2 μ M, Figure 2F) and efficiently stimulated BMP-dependent osteogenesis from C2C12 myoblasts (Figure 2G). Here, Autophinib even outperformed high-dosed BMP-4 with ca. 2-fold higher alkaline phosphatase (ALP) activity at 1 μ M compared to 50 ng/mL BMP-4 (Figure 2H). This effect did not seem to depend on basal BMP stimulation, whereas Chromenone 1 was completely inactive in the absence of BMP-4 (Figure 2I).

Although both Autophinib and Chromenone 1 performed with similar levels of potency in both BMP-dependent, morphogenic assays, we observed quite distinct phenotypes in differentiated C2C12 cells. Figure 2J illustrates that treatment with Chromenone 1 generated the same characteristic “cobblestone phenotype” as high-dosed BMP-4, whereas Autophinib seemed to induce a myotube-like phenotype. Since ALP activity is not an exclusive and definite indicator for BMP-dependent osteoblastogenesis,^{30–32} we additionally assessed a set of gene expression markers that are characteristic for an osteogenic differentiation signature. The results confirmed that despite its strong induction of *Alp*, Autophinib did not recapitulate the typical osteogenic profile of BMP-4 but suppressed all markers, including *Runx2* and *Osterix* (*Osx*) as

secondary, indirect BMP target genes and key drivers of osteoblastogenesis (Figure 2K,L). In contrast, Chromenone 1 significantly enhanced all markers, effectively potentiating basal BMP-4 signaling input at low doses (7.5 ng/mL).

To further understand why Autophinib passed all selection criteria from the BMP-dependent differentiation assays in mESCs and C2C12 cells, we profiled a panel of 14 autophinib-based 2-aminopyrimidines (Figure S3A,B). The data suggested that morphogenic activity in mESCs and C2C12 could be linked to their activities as autophagy inhibitors targeting the class III phosphatidylinositol 3-kinase (PI3K) Vps34.³³ This seemed plausible given the well-recognized roles of PI3K type of lipid kinases on BMP signaling.^{34,35} However, two distinct Vps34 inhibitor chemotypes (i.e., SAR405 and Vps34-IN1)^{36,37} neither shared this profile nor induced any of the osteogenic and BMP-dependent differentiation markers (Figure S3C–F). We postulated that a possible contributing factor for Autophinib's activity could also derive from its pronounced GSK3 β inhibition (IC₅₀ = 2 nM).³³ Canonical Wnt signaling via GSK3 β inhibition is a well-recognized synergistic contribution to BMP-driven *Alp* and *Runx2* expression during osteoblastogenesis.³⁸ Indeed, the reference GSK3 β inhibitors BIO and CHIR-99021 exhibited the same ALP activation profile and phenotype in C2C12 cells as Autophinib (Figure S3H,I). None of the compounds were able to stimulate BMP signaling in two different BMP-response element (BRE) reporters (Figure S3J). Autophinib also did not activate TGF β or Activin A but Wnt/ β -Catenin signaling, the latter of which is characteristic for GSK3 β inhibition (Figure S3K,L).³⁹ Importantly, BIO and CHIR as GSK3 β inhibitors would not have been captured as hits (i.e., >2-fold the SD) from the primary mESC assay (see Figure S3G).

Together, we demonstrate the successful filtering of screening hits in a cascade of orthogonal validation assays and identified Vps34/GSK3 β -targeting autophagy inhibitors as potential false-positives. Early assessment of C2C12-derived phenotypes, osteogenic gene expression, and signaling pathway assay profiling present effective means to confirm genuine and selective activity on BMP. Following this procedure, Chromenone 1 could be fully validated as a novel osteogenic BMP activator chemotype and was moved forward to explore its potential as a valuable chemical biology tool for BMP signaling.

Chromenone SAR Analysis Defines Pharmacophoric Features as Osteogenic BMP Potentiators. Next, we synthesized a small series of Chromenone 1 analogues according to our established procedures for this compound class,⁴⁰ mainly focusing on the 2- and 3-positions of the 4H-chromen-4-one scaffold (see R¹ and R², Figure 3A). A total of 29 derivatives were profiled in both of the BMP-dependent assays (Figure 3B). The data showed that the 3-substituent was quite essential for activity since unsubstituted 12 (or 16–18) had no effect as well as compound 2 (Chromenone 2), only lacking the *p*-trifluoromethyl moiety. Similarly, replacement of *p*-trifluoromethyl by an electron-donating group (i.e., *p*-OMe, 3) or incorporation of an *m*-chloro (4) or *o*-methyl (5) group rendered the compounds inactive. The 2-position also did not tolerate many alterations as the 2-(1,2,4-triazolyl) substituent turned out essential for robust biological activities and could only be replaced by a pyrrol substituent (23), albeit with lower potency for this derivative. Neither 2-heteroalicyclic (e.g., 24, 26–29) nor larger 2-heteroaryl (e.g., 20–22) derivatives were active, suggesting that small heteroaromatic residues are

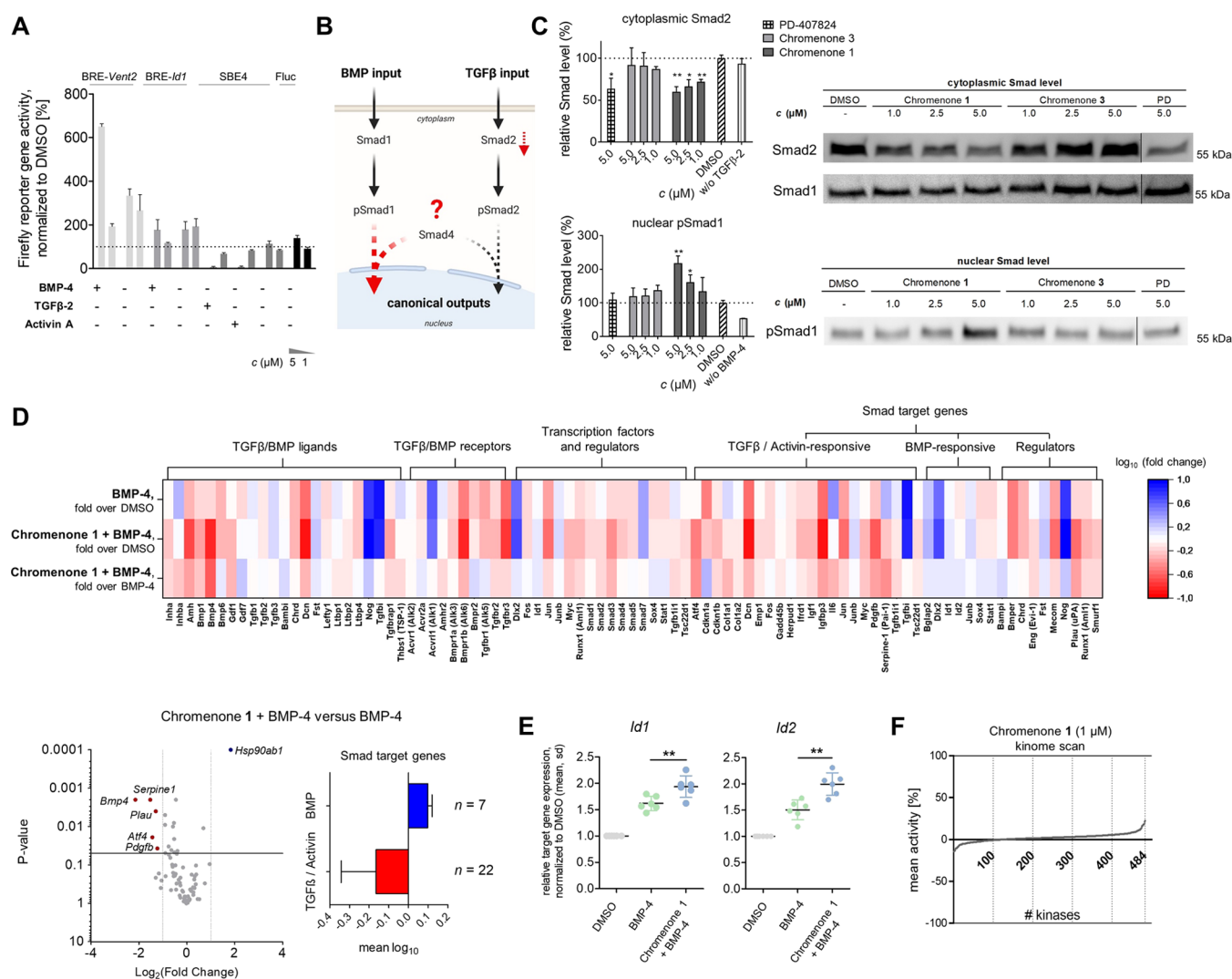


Figure 4. Combined TGFβ/BMP-Smad proteins and -PCR-array analysis reveal a negative TGFβ feedback loop for Chromenone 1. (A) Pathway selectivity profiles of Chromenone 1 on BRE-*luc* and SBE4-*luc* reporters in transiently transfected 293T cells after 22 h of co-treatment with BMP-4, TGFβ-2, or Activin A (each 10 ng/mL); data are normalized to DMSO (=100%) and shown as mean ± SD ($n \geq 3$); unspecific compound activities were excluded using a constitutively active *Fluc*-reporter as control. (B, C) Chromenone 1 decreased cytosolic TGFβ-Smad2, thereby enhancing nuclear BMP-Smad1: fractionation and quantification (Western Blot) of cytosolic Smads in C2C12 cells after 24 h compound exposure together with TGFβ-2 (10 ng/mL); nuclear (phospho)-Smad1 levels were analyzed after an additional 30 min low-dosed BMP-4 stimulus (2 ng/mL); data are normalized to DMSO and shown as mean ± SD; statistical analysis: unpaired, one-tailed *t*-test ($*p < 0.01$, $**p < 0.001$). (D) TGFβ/BMP pathway gene expression analysis with RT² Profiler PCR-Array (Qiagen) in C2C12 cells: after 24 h treatments with DMSO, BMP-4 (7.5 ng/mL), or Chromenone 1/BMP-4 (1 μM/7.5 ng/mL), the cells were lysed and RNA isolated for microarray analysis; heatmap visualization (OriginLab) shows gene expression data of 84 transcripts, sorted according to their pathway functions (log₁₀-fold changes, $n = 3$); the Volcano plot compares Chromenone 1/BMP-4 co-treatment with BMP-4 alone and indicates significantly regulated transcripts; *p*-values were calculated with a *t*-test; bar graph summarizes the mean up- and downregulation of all BMP (blue)- and TGFβ/Activin (red)-dependent Smad target genes. (E) Relative quantification of *Id1* and *Id2* gene expression upon BMP-4 (7.5 ng/mL) and Chromenone 1/BMP-4 (1 μM/7.5 ng/mL) treatments of C2C12 cells for 24 h; data are shown as mean ± SD ($n = 6$) and normalized to DMSO vehicle; Statistical analysis was performed with an unpaired two-tailed *t*-test ($*p < 0.05$, $**p < 0.01$; $***p < 0.001$). (F) *In vitro* kinome-wide profiling of Chromenone 1 (1 μM), covering the activity of 484 kinases.

preferred for the desired BMP activation. Additional combinations included variations in the 6- and 7-position (e.g., chromenones 7–11) but were not active.

Although we did not test a vast number of derivatives, distinct pharmacophoric features emerged consisting of a 4*H*-chromen-4-one scaffold with a small-sized heteroaryl substituent in 2-position and an electron-deficient aromatic group in 3-position. These data provide a solid foundation for hit optimization in the future.

However, at this point already, the 3-(*p*-phenyl) derivative (Chromenone 2) and the 2-(1,2,4-triazolyl)-lacking derivative (Chromenone 3) served as structurally closely related analogues that can be used as valuable negative controls for biological profiling and subsequent mechanistic studies (Figure 3C). The data shown in Figure 3 underscore these qualities and summarize their activity profiles as BMP potentiators on BRE-*luc* reporters (Figure 3D) and C2C12 differentiation (Figure 3E). Having this set of active and inactive chromenones in hand, we next tested whether Chromenone

1 also stimulates osteogenesis and osteoblast maturation in a human cell context. Indeed, Chromenone 1, but not its inactive analogue 3, efficiently enhanced BMP-4-induced mineralization of human osteoblastic SaOS-2 cells at low doses (i.e., 25 nM, Figure 3F). The same trend was observed when using BMP-2, although the effect was not significant (Figure S5).

Chromenones Potentiate BMP Signaling via TGF β Feedback Loops. Next, we questioned how the newly introduced chromenones potentiated BMP signaling. Figure 4A illustrates that Chromenone 1 effectively activated the BRE-*Vent2* and *-Id1* reporters, while the TGF β -specific Smad-binding element (SBE) reporter response was inhibited upon stimulation with TGF β and Activin A. We hypothesized that these activities might be directly connected through Smad4 (Figure 4B). Since Smad4 serves as a co-Smad for both the TGF β -Smads2,3 and the BMP-Smads1,5,9, a reduced amount of TGF β -Smads would leave more Smad4 for the BMP-Smads to be transported to the nucleus. Such a mechanism was suggested for PD-407824 (PD) via checkpoint kinase-1 (CHK1) inhibition leading to a p21-CDK9-mediated degradation of Smad2,3.⁹ Indeed, we found that co-treatment with Chromenone 1 and TGF β -2 for 24 h decreased cytoplasmic Smad2 levels in C2C12 cells while Smad1 remained unchanged (Figures 4C and S6). Next, we tested the consequences of this TGF β -Smad reduction and a putatively increased Smad4 availability on canonical nuclear BMP outputs. To do this, the cells were additionally stimulated with BMP-4 for 30 min after 24 h pre-incubation with Chromenone 1 and TGF β -2. Activation of BMP-Smads was significantly enhanced as observed by a dose-dependent increase in nuclear phospho-Smad1 levels (Figures 4C and S6). The BMP-inactive negative control Chromenone 3 did not significantly influence cytoplasmic or nuclear Smad levels under any conditions. However, PD turned out to only decrease Smad2 levels without enhancing phosphorylated nuclear Smad1 levels.

These results pointed at a BMP potentiating effect for Chromenone 1, triggered by a predominant downregulation of TGF β -Smads, leaving more Smad4 for translocating BMP-Smads to the nucleus. If this is the case, one would expect a differential transcriptional profile of TGF β -Smad- and BMP-Smad-target genes. Smad2,3-dependent gene expression should rather be downregulated, whereas Smad1,5,8-dependent transcripts would be upregulated. To substantiate this hypothesis, we determined an expression profile of 84 TGF β /BMP pathway-specific mRNAs by qPCR during the initial phase of BMP-dependent C2C12 differentiation (Figure 4D). The heatmap data revealed that Chromenone 1 clearly upregulated Smad target genes of BMP ($n = 7$) while those for TGF β ($n = 22$) were downregulated. Interestingly, it did not dramatically alter the overall BMP-4 expression signature, supporting the compounds' characteristics as a BMP potentiator molecule that does not perturb the quality of BMP signaling outputs. The Volcano plot reinforced that particularly TGF β -related transcripts were significantly affected (i.e., *Hsp90ab1*, *Serpine1*, *Atf4*, *Pdgfb*, *Plau*). A pronounced downregulation of *Bmp4* expression most likely reflects a cellular response to the strong amplifying effect of Chromenone 1 on BMP-4 signaling. The subtle increases in BMP target gene expression were confirmed by the observed effects on *Id1/2* by separate qPCR experiments (Figure 4E).

Since Chromenone 1 appeared to potentiate BMP signaling outputs via reduced TGF β -Smads in a distinct manner compared to PD-407824, a kinome-wide inhibition profile was determined (Figure 4E). Strikingly, Chromenone 1 did not inhibit any of the 484 tested kinases to a significant extent, including CHK1 (=proposed target of PD-407824),⁹ GSK3 α/β (=targets of Autophinib)³³ or any of the MAPKs and PI3K lipid kinases that could potentially confer noncanonical effects. Likewise, none of the TGF β family receptor kinases (ALKs) were affected by Chromenone 1. Notably, clean kinome profiles are generally very welcome for newly introduced chemical probes as they imply low polypharmacology, especially in view of the herein targeted developmental signaling pathways that are typically strongly interconnected via kinase networks.⁴¹

Together, Chromenone 1 induces a BMP stimulus-dependent downregulation of canonical TGF β effectors as opposed to instant, kinase-driven mechanisms, leading to an increased availability of Smad4 for nuclear translocation and transcriptional activity of the BMP-Smads. This represents a unique profile that cannot be recapitulated by "classic" TGF β inhibitors such as SB-431542 that failed to rescue DMH-1-mediated mesodermal differentiation in the highly BMP-dependent time frame (Figure 1C). Similarly, ALK4,5 inhibition did not stimulate C2C12 osteoblastogenesis or activated BMP signaling (Figure S6C). We believe that it will be in general difficult to entirely avoid crosstalk with TGF β , merely because effectors of this pathway represent powerful regulatory feedback loops to control BMP signaling outputs. In the case of Chromenone 1, such feedbacks eventually mediate its activity as a BMP potentiator, although the direct cellular target remains to be identified.

CONCLUSIONS

The development of small-molecule cytokine mimetics represents a challenging task in drug development. Receptor (hetero)dimerization or recruitment is typically triggered and required upon cytokine binding. This process is difficult to mimic with a small molecule and rather achieved via peptide-based approaches. Only a few examples exist, including SB-247464 as a granulocyte colony-stimulating factor mimetic or the marketed thrombopoietin mimetic Eltrombopag.^{42,43} Therefore, the development of such activators oftentimes relies on the rational perturbation of well-studied pathway components. For instance, this has been realized with Bayer's HIF-PH inhibitor Molidustat that induces the expression of erythropoietin (EPO) instead of the early attempts to mimic EPO receptor engagement.^{44–46} Notably, the discovery of new-in-class modalities is further aggravated by the fact that screening approaches oftentimes rely on rather artificial cell-based assays that might not fully resemble authentic, cell/tissue-context-relevant signaling pathway biology.

Here, we introduced a novel approach to assess the BMP pathway for drug discovery. We built on lessons learned from development and devised a phenotypic, BMP-dependent, HTS-compatible assay during mesoderm patterning of embryonic stem cells to identify novel BMP activator chemotypes. Previous work highlighted distinct BMP and TGF β /Nodal contributions to mesoderm structuring toward cardiovascular fates.^{16,17} Using pathway-selective chemical probes, we could demonstrate that a temporal discrimination of BMP- and TGF β -driven stages is indeed possible. All key functional consequences of BMP perturbation could be fully

restored by exogenous BMP-4, thus allowing the search for small molecules that mimic this action.

Proof of concept was demonstrated by screening a chemical diversity set of 7000 small molecules, including a workflow that enabled robust hit validation. The false-positive class of 2-aminopyrimidines (Autophinib) served as a useful example for effective hit de-validation, identifying GSK3 β as a relevant off-target. The cooperative action of canonical BMP and Wnt via GSK3 β is well documented. As it functions as a central hub for many more pathways, targeting GSK3 β implies a risk for polypharmacology and should be avoided. We demonstrated that this is feasible by the assessment of BMP-dependent, osteogenic marker and phenotype analysis.

The herein disclosed chromenones fulfilled all desired criteria, representing a new chemotype of BMP potentiators with high potency and efficacy. Chromenone **1** exhibited a unique mode of action as it induced a pronounced, kinase-independent, negative TGF β feedback that enhanced nuclear BMP-Smad signaling outputs. Deconvolution of cellular binding partners might expose uncharted, druggable regulators of the BMP pathway in the future. Chromenone **1** and its closely related, inactive derivatives **2** and **3** will serve as valuable chemical probes for this purpose. Notably, they already expand the collection of currently available high-quality, BMP-active chemical modalities with potential therapeutic applications for various indications.

Collectively, the presented approach successfully harnessed embryonic development as an enabling technology for drug discovery. This work might spur translations to next-generation technologies involving 3D-gastruloid or organoid systems within the field of “synthetic embryology”.

EXPERIMENTAL SECTION

Chemistry. Chromenones **1–19** were described previously by our group.⁴⁰ New compounds **20–29** were synthesized according to the established procedures A, B, or C, which are outlined in the [Supporting Information](#). Detailed synthetic protocols and analytical data are provided. The HPLC purity for all synthesized compounds was >96% for biological testing.

Cell Culture. The CGR8-mESC cell line carrying a *Myh6*-GFP reporter was grown in 15 ng/mL Leukemia inhibitory factor-containing (LIF, Dortmund Protein Facility) high-glucose Dulbecco's modified Eagle's medium (DMEM) (#21969, Gibco), supplemented with 10% FBS, GlutaMAX (Gibco), nonessential amino acids (Gibco), penicillin–streptomycin (Gibco), and 0.1 mM 2-mercaptoethanol (Gibco). The cells were cultured in 0.1% gelatine-coated six-well plates and passaged after 2–3 days to maintain pluripotency of the cell culture. C2C12 cells were maintained in DMEM (#11960, Gibco) supplemented with 10% FBS and GlutaMAX (Gibco). The cells were grown until a confluency of 70% was reached to avoid spontaneous differentiation. HEK293 cell lines were maintained in complete DMEM supplemented with 10% FBS. All of the cells were incubated at 37 °C and 5% CO₂, and assay plates were incubated at 95% humidity to reduce plate edge effects caused by evaporation.

Phenotypic BMP Activator Screening Assay. Our mESC-based cardiac differentiation assay was adapted and modified for the screening of BMP activating small molecules as follows:^{22,23,28} Clear-bottom 384-well plates (Greiner) were prepared by coating with 0.1% gelatine (in PBS, 25 μ L/well) for at least 30 min at room temperature. A gelatine solution was aspirated and seeded (500 cells/well (25 μ L/well)) using a Multidrop microplate dispenser (Thermo Scientific) in a LIF-free medium to allow spontaneous differentiation (day 0). On day 3, compounds and DMSO were added to the wells in quadruplicates for primary screening (triplicates for IC₅₀ determinations) with an Echo Liquid Handler (Labcyte). DMH-1 was added in reduced serum-containing medium to reach a final concentration of

0.5 μ M DMH-1, 0.2% DMSO, and 6% FBS under all conditions with a total assay volume of 75 μ L. To monitor the BMP rescue effects under screening conditions, 10 ng/mL rh-BMP-4 was manually added to DMH-1 control wells. After treatment for 24 h, the medium was changed to complete LIF-free mESC medium and refreshed on days 7 and 9. On day 11, the cells were fixed with 4% PFA and DAPI (1:1000 of 1 mg/mL stock in PBS) for nuclear staining 20 min at room temperature. The cells were washed thrice with PBS on a Microplate washer ELx405 (BioTek), sealed with adhesive aluminum foil (nerbe plus, Winsen, Germany), and centrifuged at 500 rpm for 1 min. The clear bottom of the plates was cleaned with isopropanol before imaging on an Image Xpress MicroXL System (Molecular Devices). For screening multiple plates, the automated microplate mover Orbitor RS was employed. The entire library of 6952 compounds was screened on 79 plates, separated into five individual runs (ca. 16 plates/run), accommodating 88 compounds per plate, which left 32 wells for all controls. GFP levels and DAPI count were quantified with MetaXpress Software 6 using a multiwavelength scoring algorithm and analyzed using the parameters “mean stain integrated intensity” and “total cells”. All data are shown as mean \pm SEM of *Myh6*-GFP levels normalized to the DMH-1 induction level and cell count, unless stated otherwise. IC₅₀ values were calculated with GraphPad Prism 5 or Quattro Workflow 3.1. Cell count levels below 70% of DMH-1 were considered false positive due to cytotoxicity.

Osteoblast Differentiation Assay. C2C12 cells were seeded at a density of 2000 cells/well in DMEM, supplemented with 6% heat-inactivated FBS, GlutaMAX, and penicillin–streptomycin in 384-well plates (Greiner). The cells were grown for 16 h and compounds/DMSO were added in triplicate with the Echo Liquid Handler (Labcyte). BMP-4 was added to the wells (7.5 ng/mL) immediately after compound addition to reach a final volume of 50 μ L/well, and the plates were incubated for 72 h. To monitor cellular ALP activity, substrate-containing CDP-Star was premixed with lysis buffer (1:100) and 15 μ L of this mix was added per well. The plates were shaken for 5 min, followed by short centrifugation and incubation at room temperature in the dark. After 1 h incubation, the luminescence was measured on a Paradigm Reader (excitation 0.2 s) and data were exported to Excel. In general, the ALP activity of 7.5 ng/mL BMP-4 in DMSO was set to 100% to calculate the synergistic activity of tested compounds. The cell toxicity was analyzed for selected compounds after compound treatment (72 h) using the commercial CellTiterGlo assay (Promega). Briefly, after the medium was aspirated and the assay reagent was added, the plates were incubated for 10 min at room temperature on a plate shaker and luminescence was measured on a Paradigm Reader (Molecular Devices). ATP levels were normalized to the BMP-4 control.

Luciferase Reporter Gene Assays. HEK293T cells were transiently transfected in batch with a luciferase reporter gene containing plasmid with Lipofectamine 2000 (Invitrogen), replated after 14 h on 96-well plates (2.5 \times 10⁴ cells/well) in 1% FBS-containing DMEM for 2 h, followed by the addition of test compounds, DMSO, and the respective growth factor (10 ng/mL) in triplicate. The cells were lysed after 22 h, and the luciferase activity was measured on a Paradigm Reader (Molecular Devices) using a Dual Luciferase Assay Kit (Promega). Additionally, the compounds were tested for nonspecific luciferase modulation using a 293/Luc cell line, containing a stably expressing firefly luciferase gene.

Quantitative Real-Time PCR. To obtain the temporal mRNA expression profiles in differentiating mESCs, RNA was isolated on desired time points from at least 12 wells (384-well plate) under each condition. Osteogenic expression marker profiles were obtained from compound-treated C2C12 cells by plating 1 \times 10⁵ cells/well in 24-well plates after growth in a differentiation medium for indicated times. Typically, compounds, DMSO, and BMP-4 were added and the cells were incubated for 72 h. In general, the cells were washed, lysed, and disrupted using a syringe with a 25 g needle. RNA was isolated with the NucleoSpin RNA Kit (Macherey Nagel) or RNeasy Mini Kit (Qiagen) according to the manufacturer's protocol. cDNA was synthesized using the qScript cDNA Synthesis Kit (Quanta

Bioscience) on a PCR thermocycler and RT-qPCR was performed with Takyon SYBR Master Mix (Eurogentec) on a Lightcycler 480 (Roche). Primers were purchased from IDT (Integrated DNA Technologies, Leuven), and all sequences are listed in the Supporting Information (Table S2). For the determination of the relative gene expression, the $\Delta\Delta C_p$ method was used. All data points are shown as mean of triplicates \pm SD, normalized to DMSO unless stated otherwise.

PCR Array Analysis. After 24 h treatments, C2C12 were washed, lysed, and RNA was isolated with the RNeasy Mini Kit (Qiagen). The cDNA was synthesized using the RT² First Strand Kit (Qiagen) on a PCR thermocycler according to the manufacturer's protocol. The array was performed using the RT² SYBR Green qPCR Mastermix (Qiagen) on an RT² Profiler PCR Array (PAMM-035ZG) for Mouse TGF β /BMP Signaling Pathway.

Western Blot Analysis. C2C12 cells were cultivated in 100 mm dishes (2.5×10^6 cells/well) and treated as indicated. Subcellular fractionation was performed through a modified protocol based on Schreiber et al.⁴⁷ In brief, the cells were detached with trypsin, lysed, and washed thrice in cytoplasmic extraction buffer (10 mM 4-(2-hydroxyethyl)-1-piperazineethanesulfonic acid, HEPES, 10 mM KCl, 0.1 mM ethylenediaminetetraacetic acid (EDTA), 1 mM dithiothreitol, 0.5% Nonidet-P40, pH 7.5). Pellets containing the nuclei were lysed in nuclear extraction buffer (10 mM HEPES, 400 mM NaCl, 1 mM EDTA, 1 mM dithiothreitol, pH 7.5). All buffers contained phosphatase inhibitor cocktail (Sigma) and cComplete protease inhibitor cocktail (Roche). Protein quantification was performed with Pierce BCA Protein Assay Kit (Thermo Scientific). Protein was loaded on self-cast polyacrylamide gels containing 0.5% trichloroethanol.⁴⁸ Before blotting, the gels were illuminated with UV light for 5 min and fluorescence and luminescence signals were imaged with an Intas ChemoStar instrument. Quantification was done with LabImage 1D software, and antigen-specific luminescence intensities were normalized to total protein amount per lane.

In Vitro Osteoblast Mineralization Assay. Human SaOS-2 cells were cultured in DMEM (DMEM/F12, Sigma), supplemented with 10% FCS and 1% penicillin–streptomycin. For osteogenic differentiation, the medium was supplemented with 10 mM β -glycerophosphate, 0.2 mM ascorbic acid, and 10 nM dexamethasone. The cells were seeded in 96-well plates (8×10^3 cells/well), and the osteogenic differentiation medium was changed every 3 days with or without compounds and ascorbic acid was refreshed every day. For osteogenic induction, 2 ng/mL BMP-4 or BMP-2 was added. DMSO (0.01%) was used as a vehicle control, and the cells were incubated for 11 days. The extent of mineralization was quantified after von Kossa staining and image analysis as follows: The cell cultures were washed twice with PBS (Sigma), fixed in 4% PFA for 10 min, and washed once with water. A 5% AgNO₃ in aqua dest solution was added into the wells and the plates were exposed to sunlight for 1 h. The wells were rinsed with water and incubated with 1% 1,2,3-trihydroxybenzol for 3 min, followed by washing and addition of 5% Na₂S₂O₃ for 3 min. The wells were washed twice with EtOH and the plates were dried for microscopic imaging. For image analysis, von Kossa-stained area was quantified using black and white images and a color threshold to quantify the amount of black color with Image J. The mean value for von Kossa-stained area was quantified from at least four images for each test condition using a 100 \times magnification.

Statistical Analysis. Statistical analysis between two groups was performed with an unpaired *t*-test and a set confidence level of 95% of three replicates and $n \geq 3$ independent biological experiments unless stated otherwise. Symbols for the significance level are indicated as follows, unless stated otherwise: ns, not significant; * $p < 0.05$; ** $p < 0.01$; *** $p < 0.001$. IC₅₀ and EC₅₀ values were calculated with GraphPad Prism 5–7.

■ ASSOCIATED CONTENT

SI Supporting Information

The Supporting Information is available free of charge at <https://pubs.acs.org/doi/10.1021/acs.jmedchem.1c01800>.

Extended experimentals of key reagents and resources (Table S1), list of primer sequences (Table S2), additional experimental data on the establishment and characterization of the novel phenotypic BMP activator screening assay in mESCs (Figure S1), establishment of a BMP-dependent osteoblastic differentiation assay and characterization of BMP activator/potentiator reference compounds (Figure S2), SAR analysis and de-validation of Vps34/GSK3-targeting 2-aminopyrimidine hit class (Figure S3), de-validation of the quinolinol hit chemotype (Figure S4), *in vitro* mineralization assay in the human osteosarcoma cell line SaOS-2 (Figure S5), semiquantitative immunoblottings (Figure S6), kinase profiling of Chromenone 1 and the influence of TGF β (ALK4,5,7) inhibitor SB-431542 and the TGF β type II receptor degrader DHP-2 on osteogenesis (Figure S7), and experimental details and analytical data for all newly synthesized compounds (20–29) (PDF)

Raw and processed array data (XLSX)

Raw and processed array data (XLSX)

Molecular formula strings (CSV)

■ AUTHOR INFORMATION

Corresponding Author

Dennis Schade – Department of Pharmaceutical and Medicinal Chemistry, Institute of Pharmacy, Christian-Albrechts-University of Kiel, 24118 Kiel, Germany; Max-Planck-Institute of Molecular Physiology, 44227 Dortmund, Germany; Partner Site Kiel, DZHK, German Center for Cardiovascular Research, 24105 Kiel, Germany; orcid.org/0000-0002-5515-1821; Phone: (+49) 431 880 1176; Email: schade@pharmazie.uni-kiel.de; Fax: (+49) 431 880 1352

Authors

Fabian Wesseler – Faculty of Chemistry and Chemical Biology, Technical University Dortmund, 44227 Dortmund, Germany; Compound Management and Screening Center, 44227 Dortmund, Germany; Department of Pharmaceutical and Medicinal Chemistry, Institute of Pharmacy, Christian-Albrechts-University of Kiel, 24118 Kiel, Germany

Daniel Riege – Department of Pharmaceutical and Medicinal Chemistry, Institute of Pharmacy, Christian-Albrechts-University of Kiel, 24118 Kiel, Germany

Mahesh Puthanveedu – Faculty of Chemistry and Chemical Biology, Technical University Dortmund, 44227 Dortmund, Germany; Max-Planck-Institute of Molecular Physiology, 44227 Dortmund, Germany

Jonas Halver – Faculty of Chemistry and Chemical Biology, Technical University Dortmund, 44227 Dortmund, Germany

Eva Müller – Department of Orthopedic Surgery, Otto-von-Guericke University, 39120 Magdeburg, Germany

Jessica Bertrand – Department of Orthopedic Surgery, Otto-von-Guericke University, 39120 Magdeburg, Germany

Andrey P. Antonchick – Faculty of Chemistry and Chemical Biology, Technical University Dortmund, 44227 Dortmund, Germany; Max-Planck-Institute of Molecular Physiology, 44227 Dortmund, Germany; Department of Chemistry and Forensics, College of Science and Technology, Nottingham Trent University, NG11 8NS Nottingham, United Kingdom; orcid.org/0000-0003-0435-9443

Sonja Sievers – Compound Management and Screening Center, 44227 Dortmund, Germany; Max-Planck-Institute of Molecular Physiology, 44227 Dortmund, Germany

Herbert Waldmann – Faculty of Chemistry and Chemical Biology, Technical University Dortmund, 44227 Dortmund, Germany; Max-Planck-Institute of Molecular Physiology, 44227 Dortmund, Germany; orcid.org/0000-0002-9606-7247

Complete contact information is available at:

<https://pubs.acs.org/10.1021/acs.jmedchem.1c01800>

Author Contributions

D.S. conceived and designed the project. F.W., D.R., J.H., J.B., and E.M. performed the biological experiments. M.P. performed the chemical synthesis. All of the authors analyzed and discussed the results. F.W. and D.S. prepared the manuscript.

Notes

The authors declare no competing financial interest.

ACKNOWLEDGMENTS

The authors are very grateful to Mark Mercola (Stanford University) for sharing materials and his helpful suggestions and discussions related to the manuscript. They also thank the Dortmund Protein Chemistry Facility for providing high-quality LIF and Christiane Pfaff and Carina Birke for excellent technical assistance at the COMAS screening facility. Petra Köster, Meike Wichmann, and Tanja Schuh are gratefully acknowledged for technical support with biological experiments. The authors also thank Michael Schulz for his help with the FACS instrument. This work was supported by funds from the German Federal Ministry of Science and Education (BMBF, grant 131605).

ABBREVIATIONS

AcA, activin A; ALK, activin receptor-like kinase; ALP, alkaline phosphatase; BMP, bone morphogenetic protein; BMPR, BMP receptor; BraT, brachyury T; BRE, BMP-responsive element; Cer, cerberus; CHK-1, checkpoint kinase 1; Col1a1, collagen type I α 1; DHP, 1,4-dihydropyridine; DM, dorsomorphin; DMH-1, dorsomorphin-homologue 1; ESC, embryonic stem cell; FBS, fetal bovine serum; GF, growth factor; GSK3, glycogen synthase kinase 3; Id, inhibitor of DNA binding; ITD-1, inducer of TGFBR-II degradation-1; LIF, leukemia inhibitory factor; Luc, luciferase; MAPK, mitogen-activated protein kinase; Mef2c, myocyte-specific enhancer factor 2C; mESC, murine embryonic stem cell; Mesp1, mesoderm posterior 1 homolog; Myh6, myosin heavy chain-6; Ocn, osteocalcin; Osx, osterix; PD, PD407824; PI3K, phosphoinositol-3 kinase; PSC, pluripotent stem cell; RGA, reporter gene assay; Runx2, runt-related transcription factor 2 (CBF- α -1); SBE, SMAD-binding element; SD, standard deviation; SEM, standard error of mean; TGF β , transforming growth factor- β ; Tnnt2, Troponin T2

REFERENCES

(1) Salazar, V. S.; Gamer, L. W.; Rosen, V. BMP signalling in skeletal development, disease and repair. *Nat. Rev. Endocrinol.* **2016**, *12*, 203–221.
(2) Wagner, D. O.; Sieber, C.; Bhushan, R.; Börgermann, J. H.; Graf, D.; Knaus, P. BMPs: From bone to body morphogenetic proteins. *Sci. Signaling* **2010**, *3*, No. mrl.

(3) Nohe, A.; Keating, E.; Knaus, P.; Petersen, N. O. Signal transduction of bone morphogenetic protein receptors. *Cell. Signalling* **2004**, *16*, 291–299.

(4) Heldin, C. H.; Miyazono, K.; ten Dijke, P. TGF-beta signalling from cell membrane to nucleus through SMAD proteins. *Nature* **1997**, *390*, 465–471.

(5) Hollnagel, A.; Oehlmann, V.; Heymer, J.; Ruther, U.; Nordheim, A. Id genes are direct targets of bone morphogenetic protein induction in embryonic stem cells. *J. Biol. Chem.* **1999**, *274*, 19838–19845.

(6) Lowery, J. W.; Rosen, V. Bone morphogenetic protein-based therapeutic approaches. *Cold Spring Harbor Perspect. Biol.* **2018**, *10*, No. a022327.

(7) Carreira, A. C.; Lojudice, F. H.; Halcsik, E.; Navarro, R. D.; Sogayar, M. C.; Granjeiro, J. M. Bone morphogenetic proteins: Facts, challenges, and future perspectives. *J. Dent. Res.* **2014**, *93*, 335–345.

(8) Genthe, J. R.; Min, J.; Farmer, D. M.; Shelat, A. A.; Grenet, J. A.; Lin, W.; Finkelstein, D.; Vrijens, K.; Chen, T.; Guy, R. K.; Clements, W. K.; Roussel, M. F. Ventromorphins: A new class of small molecule activators of the canonical BMP signaling pathway. *ACS Chem. Biol.* **2017**, *12*, 2436–2447.

(9) Feng, L.; Cook, B.; Tsai, S.-Y.; Zhou, T.; LaFlamme, B.; Evans, T.; Chen, S. Discovery of a small-molecule BMP sensitizer for human embryonic stem cell differentiation. *Cell Rep.* **2016**, *15*, 2063–2075.

(10) Larraufie, M. H.; Gao, X.; Xia, X.; Devine, P. J.; Kallen, J.; Liu, D.; Michaud, G.; Harsch, A.; Savage, N.; Ding, J.; Tan, K.; Mihalic, M.; Roggo, S.; Canham, S. M.; Bushell, S. M.; Krastel, P.; Gao, J.; Izaac, A.; Altinoglu, E.; Lustenberger, P.; Salcius, M.; Harbinski, F.; Williams, E. T.; Zeng, L.; Loureiro, J.; Cong, F.; Fryer, C. J.; Klickstein, L.; Tallarico, J. A.; Jain, R. K.; Rothman, D. M.; Wang, S. Phenotypic screen identifies calcineurin-sparing FK506 analogs as BMP potentiators for treatment of acute kidney injury. *Cell Chem. Biol.* **2021**, *28*, 1271–1282.

(11) Rao, J.; Pfeiffer, M. J.; Frank, S.; Adachi, K.; Piccini, I.; Quaranta, R.; Araúzo-Bravo, M.; Schwarz, J.; Schade, D.; Leidel, S.; Schöler, H. R.; Seebohm, G.; Greber, B. Stepwise clearance of repressive roadblocks drives cardiac induction in human ESCs. *Cell Stem Cell* **2016**, *18*, 554–556.

(12) Qi, X.; Li, T.-G.; Hao, J.; Hu, J.; Wang, J.; Simmons, H.; Miura, S.; Mishina, Y.; Zhao, G.-Q. BMP4 supports self-renewal of embryonic stem cells by inhibiting mitogen-activated protein kinase pathways. *Proc. Natl. Acad. Sci. U.S.A.* **2004**, *101*, 6027–6032.

(13) Pfeiffer, M. J.; Quaranta, R.; Piccini, I.; Fell, J.; Rao, J.; Ropke, A.; Seebohm, G.; Greber, B. Cardiogenic programming of human pluripotent stem cells by dose-controlled activation of EOMES. *Nat. Commun.* **2018**, *9*, No. 440.

(14) Birket, M. J.; Ribeiro, M. C.; Verkerk, A. O.; Ward, D.; Leitoguinho, A. R.; den Hartogh, S. C.; Orlova, V. V.; Devalla, H. D.; Schwach, V.; Bellin, M.; Passier, R.; Mummery, C. L. Expansion and patterning of cardiovascular progenitors derived from human pluripotent stem cells. *Nat. Biotechnol.* **2015**, *33*, 970–979.

(15) Schade, D.; Plowright, A. T. Medicinal chemistry approaches to heart regeneration. *J. Med. Chem.* **2015**, *58*, 9451–9479.

(16) Cai, W.; Albini, S.; Wei, K.; Willems, E.; Guzzo, R. M.; Tsuda, M.; Giordani, L.; Spiering, S.; Kurian, L.; Yeo, G. W.; Puri, P. L.; Mercola, M. Coordinate Nodal and BMP inhibition directs Baf60c-dependent cardiomyocyte commitment. *Genes Dev.* **2013**, *27*, 2332–2344.

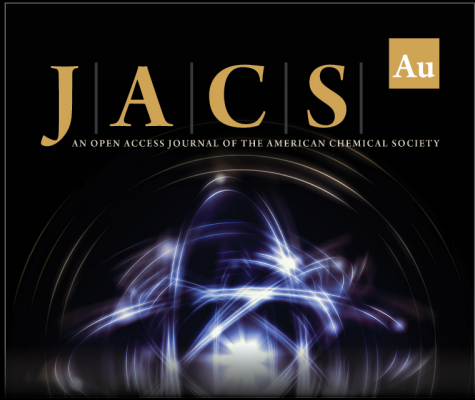
(17) Cunningham, T. J.; Yu, M. S.; McKeithan, W. L.; Spiering, S.; Carrette, F.; Huang, C. T.; Bushway, P. J.; Tierney, M.; Albini, S.; Giacca, M.; Mano, M.; Puri, P. L.; Sacco, A.; Ruiz-Lozano, P.; Riou, J. F.; Umbhauer, M.; Duyster, G.; Mercola, M.; Colas, A. R. Id genes are essential for early heart formation. *Genes Dev.* **2017**, *31*, 1325–1338.

(18) Yuasa, S.; Itabashi, Y.; Koshimizu, U.; Tanaka, T.; Sugimura, K.; Kinoshita, M.; Hattori, F.; Fukami, S.; Shimazaki, T.; Ogawa, S.; Okano, H.; Fukuda, K. Transient inhibition of BMP signaling by Noggin induces cardiomyocyte differentiation of mouse embryonic stem cells. *Nat. Biotechnol.* **2005**, *23*, 607–611.


- (19) Nosedá, M.; Peterkin, T.; Simoes, F. C.; Patient, R.; Schneider, M. D. Cardiopoietic factors: extracellular signals for cardiac lineage commitment. *Circ. Res.* **2011**, *108*, 129–152.
- (20) Yu, P. B.; Hong, C. C.; Sachidanandan, C.; Babitt, J. L.; Deng, D. Y.; Hoyng, S. A.; Lin, H. Y.; Bloch, K. D.; Peterson, R. T. Dorsomorphin inhibits BMP signals required for embryogenesis and iron metabolism. *Nat. Chem. Biol.* **2008**, *4*, 33–41.
- (21) Hao, J.; Ho, J. N.; Lewis, J. A.; Karim, K. A.; Daniels, R. N.; Gentry, P. R.; Hopkins, C. R.; Lindsley, C. W.; Hong, C. C. In vivo structure-activity relationship study of dorsomorphin analogues identifies selective VEGF and BMP inhibitors. *ACS Chem. Biol.* **2010**, *5*, 245–253.
- (22) Willems, E.; Cabral-Teixeira, J.; Schade, D.; Cai, W.; Reeves, P.; Bushway, P. J.; Lanier, M.; Walsh, C.; Kirchhausen, T.; Izipisua, B. J. C.; Cashman, J.; Mercola, M. Small molecule-mediated TGF- β type II receptor degradation promotes cardiomyogenesis in embryonic stem cells. *Cell Stem Cell* **2012**, *11*, 242–252.
- (23) Schade, D.; Lanier, M.; Willems, E.; Okolotowicz, K.; Bushway, P.; Wahlquist, C.; Gilley, C.; Mercola, M.; Cashman, J. R. Synthesis and SAR of *b*-annulated 1,4-dihydropyridines define cardiomyogenic compounds as novel inhibitors of TGF β signaling. *J. Med. Chem.* **2012**, *55*, 9946–9957.
- (24) Piccolo, S.; Agius, E.; Leyns, L.; Bhattacharyya, S.; Grunz, H.; Bouwmeester, T.; De Robertis, E. M. The head inducer Cerberus is a multifunctional antagonist of Nodal, BMP and Wnt signals. *Nature* **1999**, *397*, 707–710.
- (25) Engers, D. W.; Frist, A. Y.; Lindsley, C. W.; Hong, C. C.; Hopkins, C. R. Synthesis and structure-activity relationships of a novel and selective bone morphogenetic protein receptor (BMP) inhibitor derived from the pyrazolo[1.5-*a*]pyrimidine scaffold of dorsomorphin: the discovery of ML347 as an ALK2 versus ALK3 selective MLPCN probe. *Bioorg. Med. Chem. Lett.* **2013**, *23*, 3248–3252.
- (26) Xie, C.; Jiang, W.; Lacroix, J. J.; Luo, Y.; Hao, J. Insight into molecular mechanism for activin A-induced bone morphogenetic protein signaling. *Int. J. Mol. Sci.* **2020**, *21*, No. 6498.
- (27) Olsen, O. E.; Hella, H.; Elsaadi, S.; Jacobi, C.; Martinez-Hackert, E.; Holien, T. Activins as dual specificity TGF- β family molecules: SMAD-activation via activin- and BMP-type I receptors. *Biomolecules* **2020**, *10*, No. 519.
- (28) Halver, J.; Wenzel, K.; Sendker, J.; Carrillo Garcia, C.; Erdelmeier, C.; Willems, E.; Mercola, M.; Symma, N.; Köneman, S.; Koch, E.; Hensel, A.; Schade, D. Crataegus Extract WS1442 Stimulates cardiomyogenesis and angiogenesis from stem cells: A possible new pharmacology for hawthorn? *Front. Pharmacol.* **2019**, *10*, No. 1357.
- (29) Vrijens, K.; Lin, W.; Cui, J.; Farmer, D.; Low, J.; Pronier, E.; Zeng, F.-Y.; Shelat, A. A.; Guy, K.; Taylor, M. R.; Chen, T.; Roussel, M. F. Identification of small molecule activators of BMP signaling. *PLoS One* **2013**, *8*, No. e59045.
- (30) Zhang, J.; Zhang, W.; Dai, J.; Wang, X.; Shen, S. G. Overexpression of Dlx2 enhances osteogenic differentiation of BMSCs and MC3T3-E1 cells via direct upregulation of Osteocalcin and Alp. *Int. J. Oral Sci.* **2019**, *11*, No. 12.
- (31) Hassel, S.; Yakymovych, M.; Hellman, U.; Ronnstrand, L.; Knaus, P.; Souchelnytskyi, S. Interaction and functional cooperation between the serine/threonine kinase bone morphogenetic protein type II receptor with the tyrosine kinase stem cell factor receptor. *J. Cell. Physiol.* **2006**, *206*, 457–467.
- (32) Fukuda, T.; Kokabu, S.; Ohte, S.; Sasanuma, H.; Kanomata, K.; Yoneyama, K.; Kato, H.; Akita, M.; Oda, H.; Katagiri, T. Canonical Wnts and BMPs cooperatively induce osteoblastic differentiation through a GSK3 β -dependent and β -catenin-independent mechanism. *Differentiation* **2010**, *80*, 46–52.
- (33) Robke, L.; Laraia, L.; Carnero Corrales, M. A.; Konstantinidis, G.; Muroi, M.; Richters, A.; Winzker, M.; Engbring, T.; Tomassi, S.; Watanabe, N.; Osada, H.; Rauh, D.; Waldmann, H.; Wu, Y. W.; Engel, J. Phenotypic identification of a novel autophagy inhibitor chemotype targeting lipid kinase VPS34. *Angew. Chem., Int. Ed.* **2017**, *56*, 8153–8157.
- (34) Viñals, F.; Lopez-Rovira, T.; Rosa, J. L.; Ventura, F. Inhibition of PI3K/p70 S6K and p38 MAPK cascades increases osteoblastic differentiation induced by BMP-2. *FEBS Lett.* **2002**, *510*, 99–104.
- (35) Ghosh-Choudhury, N.; Abboud, S. L.; Nishimura, R.; Celeste, A.; Mahimainathan, L.; Choudhury, G. G. Requirement of BMP-2-induced phosphatidylinositol 3-kinase and Akt serine/threonine kinase in osteoblast differentiation and Smad-dependent BMP-2 gene transcription. *J. Biol. Chem.* **2002**, *277*, 33361–33388.
- (36) Ronan, B.; Flamand, O.; Vescovi, L.; Dureuil, C.; Durand, L.; Fassy, F.; Bachelot, M. F.; Lambertson, A.; Mathieu, M.; Bertrand, T.; Marquette, J. P.; El-Ahmad, Y.; Filoche-Romme, B.; Schio, L.; Garcia-Echeverria, C.; Goulaouic, H.; Pasquier, B. A highly potent and selective Vps34 inhibitor alters vesicle trafficking and autophagy. *Nat. Chem. Biol.* **2014**, *10*, 1013–1019.
- (37) Bago, R.; Malik, N.; Munson, M. J.; Prescott, A. R.; Davies, P.; Sommer, E.; Shpiro, N.; Ward, R.; Cross, D.; Ganley, I. G.; Alessi, D. R. Characterization of VPS34-IN1, a selective inhibitor of Vps34, reveals that the phosphatidylinositol 3-phosphate-binding SGK3 protein kinase is a downstream target of class III phosphoinositide 3-kinase. *Biochem. J.* **2014**, *463*, 413–427.
- (38) Rodríguez-Carballo, E.; Ulsamer, A.; Susperregui, A. R.; Manzanares-Cespedes, C.; Sanchez-Garcia, E.; Bartrons, R.; Rosa, J. L.; Ventura, F. Conserved regulatory motifs in osteogenic gene promoters integrate cooperative effects of canonical Wnt and BMP pathways. *J. Bone Miner. Res.* **2011**, *26*, 718–729.
- (39) Sato, N.; Meijer, L.; Skaltsounis, L.; Greengard, P.; Brivanlou, A. H. Maintenance of pluripotency in human and mouse embryonic stem cells through activation of Wnt signaling by a pharmacological GSK-3-specific inhibitor. *Nat. Med.* **2004**, *10*, 55–63.
- (40) Samanta, R.; Narayan, R.; Bauer, J. O.; Strohmann, C.; Sievers, S.; Antonchick, A. P. Oxidative regioselective amination of chromones exposes potent inhibitors of the hedgehog signaling pathway. *Chem. Commun.* **2015**, *51*, 925–928.
- (41) Arrowsmith, C. H.; Audia, J. E.; Austin, C.; Baell, J.; Bennett, J.; Blagg, J.; Bountra, C.; Brennan, P. E.; Brown, P. J.; Bunnage, M. E.; Buser-Doepner, C.; Campbell, R. M.; Carter, A. J.; Cohen, P.; Copeland, R. A.; Cravatt, B.; Dahlin, J. L.; Dhanak, D.; Am, E.; Frederiksen, M.; Frye, S. V.; Gray, N.; Grimshaw, C. E.; Hepworth, D.; Howe, T.; Huber, K. V.; Jin, J.; Knapp, S.; Kotz, J. D.; Kruger, R. G.; Lowe, D.; Mader, M. M.; Marsden, B.; Mueller-Fahrnow, A.; Müller, S.; O'Hagan, R. C.; Overington, J. P.; Owen, S.; Rosenberg, S. H.; Roth, B.; Ross, R.; Schapira, M.; Schreiber, S. L.; Shoichet, B.; Sundström, M.; Superti-Furga, G.; Taunton, J.; Toledo-Sherman, L.; Walpole, C.; Walters, M. A.; Willson, T. M.; Workman, P.; Young, R. N.; Zuercher, W. J. The promise and peril of chemical probes. *Nat. Chem. Biol.* **2015**, *11*, 536–541.
- (42) Tian, S. S.; Lamb, P.; King, A. G.; Miller, S. G.; Kessler, L.; Luengo, J. I.; Averill, L.; Johnson, R. K.; Gleason, J. G.; Pelus, L. M.; Dillon, S. B.; Rosen, J. A small, nonpeptidyl mimic of granulocyte-colony-stimulating factor [see comments]. *Science* **1998**, *281*, 257–259.
- (43) Duffy, K. J.; Erickson-Miller, C. L. The Discovery of Eltrombopag, An Orally Bioavailable TpoR Agonist. In *Target Validation in Drug Discovery*; Metcalf, B. W.; Dillon, S., Eds.; Academic Press, 2007; pp 241–254.
- (44) Beck, H.; Jeske, M.; Thede, K.; Stoll, F.; Flamme, I.; Akbaba, M.; Erguden, J. K.; Karig, G.; Keldenich, J.; Oehme, F.; Miltzer, H. C.; Hartung, I. V.; Thuss, U. Discovery of Molidustat (BAY 85-3934): A small-molecule oral HIF-prolyl hydroxylase (HIF-PH) inhibitor for the treatment of renal anemia. *ChemMedChem* **2018**, *13*, 988–1003.
- (45) Livnah, O.; Stura, E. A.; Johnson, D. L.; Middleton, S. A.; Mulcahy, L. S.; Wrighton, N. C.; Dower, W. J.; Jolliffe, L. K.; Wilson, I. A. Functional mimicry of a protein hormone by a peptide agonist: the EPO receptor complex at 2.8 Å. *Science* **1996**, *273*, 464–471.
- (46) Qureshi, S. A.; Kim, R. M.; Konteatis, Z.; Biazzo, D. E.; Motamedi, H.; Rodrigues, R.; Boice, J. A.; Calaycay, J. R.; Bednarek, M. A.; Griffin, P.; Gao, Y. D.; Chapman, K.; Mark, D. F. Mimicry of erythropoietin by a nonpeptide molecule. *Proc. Natl. Acad. Sci. U.S.A.* **1999**, *96*, 12156–12161.


(47) Schreiber, E.; Matthias, P.; Muller, M. M.; Schaffner, W. Rapid detection of octamer binding proteins with 'mini-extracts', prepared from a small number of cells. *Nucleic Acids Res.* **1989**, *17*, No. 6419.


(48) Ladner, C. L.; Edwards, R. A.; Schriemer, D. C.; Turner, R. J. Identification of trichloroethanol visualized proteins from two-dimensional polyacrylamide gels by mass spectrometry. *Anal. Chem.* **2006**, *78*, 2388–2396.



JACS Au
AN OPEN ACCESS JOURNAL OF THE AMERICAN CHEMICAL SOCIETY

 Editor-in-Chief
Prof. Christopher W. Jones
Georgia Institute of Technology, USA

Open for Submissions 

pubs.acs.org/jacsau  ACS Publications
Most Trusted. Most Cited. Most Read.